^{209}Bi NMR and NQR investigation of the small-gap semiconductor $Ce_3Bi_4Pt_3$

A. P. Reyes,* R. H. Heffner, P. C. Canfield,† J. D. Thompson, and Z. Fisk
Los Alamos National Laboratory, Los Alamos, New Mexico 87545
(Received 14 February 1994)

We report measurements of the temperature dependence of the ^{209}Bi nuclear quadrupole resonance frequency ν_Q, the Knight shift K, and the spin-lattice relaxation rate $1/T_1$ in the small-gap semiconductor $Ce_3Bi_4Pt_3$ between 1.8 and 300 K. Corresponding measurements also are reported for the nonmagnetic metallic isomorph $La_3Bi_4Pt_3$. The ν_Q data in the Ce compound show a characteristic departure from metallic-to-insulating behavior when the sample is cooled below $T_M = 80$ K, the temperature of the susceptibility maximum, attributable to a loss of low-frequency vibrational modes in the insulating state. The Knight shift has both isotropic and axial components; this anisotropy originates from the presence of Ce via a transferred hyperfine coupling between Ce $4f$ and conduction electrons. An s-f exchange constant ≥ 0.4 eV is found, consistent with hybridization in other rare-earth intermetallic compounds. A change in the scaling between the susceptibility and both the isotropic and axial Knight shifts at temperature T_M provides evidence that hybridization between the Ce $4f$ orbitals and the conduction electrons is responsible for the gap structure. The temperature dependence of the $1/T_1$ data is consistent with a model electronic density of states possessing a temperature-independent gap δ of 180 K and a bandwidth of the order of 1600 K. The temperature dependence of $1/T_1$ can also be fit well with a temperature-dependent gap with $\delta(0)$ also ≈ 180 K.

I. INTRODUCTION

The compound $Ce_3Bi_4Pt_3$ (hereafter referred to as Ce343) is one of about a dozen small-gap semiconducting compounds involving either rare-earth or actinide metals.[1] Most of these semiconductors possess a cubic structure, and the behavior of their lattice parameters suggests a mixed-valence state for the f electrons. The dc susceptibility typically increases with temperature, passes through a maximum, and then falls again, exhibiting local-moment behavior at high temperatures with nearly the full local-moment value. This behavior is characteristic of dense Kondo systems, where the reduction in the susceptibility at low temperatures is produced by the hybridization of the local moments with the conduction electrons. In some materials, this hybridization is assumed to produce an energy gap, which is usually less than 1000 K.[1] The conditions for gapping the entire Fermi surface, just two electrons per f site and the intersection of the f level with only one conduction band at the Fermi surface, are most easily met in cubic materials.

Several issues are of current interest regarding these small-gap semiconductors. First, although the gap has been assumed to arise from hybridization, it is important to find good experimental evidence for this hypothesis. Second, the magnitudes of both the charge (δ_c) and spin (δ_s) gaps need to be established. For example, strong-coupling models[2] predict that the ratio of δ_c to δ_s is at least 1.5. Finally, the temperature dependence of the gap should be investigated, as well as whether or not there are intrinsic states within the gap.

In this paper we present nuclear magnetic and nuclear quadrupole resonance (NMR and NQR) experiments on Ce343, a cubic small-gap semiconductor with a susceptibility maximum near 80 K.[3] This susceptibility maximum leads to an estimation[3] for the Kondo temperature T_K of about 320 K. The transport gap in Ce343, as measured by resistivity, is temperature dependent, reaching a maximum of about 120 K below about 50 K.[4] By contrast, recent far-infrared reflectivity measurements report a charge gap of about 450 K, with a significant density of states below this energy.[5] Inelastic neutron scattering experiments yield a spin gap of about 150 K, and are somewhat ambiguous regarding the existence of discernible states in the gap.[6] A small linear coefficient of specific heat γ (≤ 3 mJ/mol Ce K^2) has also been measured.[3]

The nonmagnetic analog to Ce343 is $La_3Bi_4Pt_3$ (referred to here as La343), which is metallic down to 4 K.[3] The substitution of La for Ce in Ce343 decreases the low-temperature resistivity and eventually destroys the energy gap. The properties of both Ce343 and La343 are reviewed in Refs. 1 and 3.

Nuclear magnetic resonance probes the local spin density and electronic and magnetic structure of materials and can therefore yield information on the microscopic nature of these hybridization-gap systems. For example, measurements of the Knight shift have an inherent advantage over susceptibility measurements because impurities and other phases generally do not affect the Knight shift. The NMR spin-lattice relaxation rate is sensitive to the excitation of quasiparticles across the gap structure, yielding information about the spin gap. Finally, nuclear quadrupole resonance can be used to probe the charge distribution surrounding the nucleus through a measure of the local electric field gradient (EFG).

In Curie-Weiss paramagnets one can in principle observe NMR at either the magnetic- or nonmagnetic-ion site. However, the NMR at the site of the magnetic ion can be rendered unobservable by the rapid relaxation of the paramagnetic ion itself. When NMR is carried out at

the site of the nonmagnetic nuclei, such as in Ce compounds, the coupling to the $4f$ moments occurs via indirect interactions such as transferred hyperfine and dipolar fields. This poses an uncertainty in the interpretation of the data because, except for dipolar fields from well-localized moments, this coupling is hard to calculate. Moreover, the anisotropy of the local $4f$ susceptibility cannot be determined using a nonmagnetic-probe site whose symmetry differs from that of the f site. Nevertheless, because NMR is sensitive to the static and dynamic behavior of both the electrostatic and the magnetic environment of the nuclei, it is a useful probe with which to address the issues raised above concerning the small-gap semiconductors.

II. SAMPLE PREPARATION AND CHARACTERIZATION

Single crystals of Ce343 were grown from excess Bi flux.[7] X-ray diffraction results exhibited a single-phase material. Approximately 1 g of these crystals was ground and sealed in an epoxy container for the magnetic resonance experiments.

The dc susceptibility was measured using a superconducting quantum interference device (SQUID) magnetometer between 4 and 350 K and is shown in Fig. 1. The data exhibit a maximum at $T_M \sim 80$ K and a small sample-dependent Curie tail below about 30 K due to magnetic impurities, as discussed below. The smallness of the Curie tail seen for $T < 30$ K is indicative of the high sample purity, as is the increase in electrical resistivity by a factor of 1000 seen in typical samples on cooling from room temperature to 2 K. Above $T \sim 150$ K, the susceptibility data are consistent with a Curie-Weiss behavior with effective moment nearly equal to the free Ce^{3+} ion value (see Sec. IV B below).

Ce343 crystallizes in a body-centered cubic $Y_3Sb_4Au_3$ structure with $I\bar{4}3d$ symmetry. Each unit cell contains four formula units. All Ce and Pt atoms occupy one unique crystallographic site with a fourfold inversion symmetry, forming an intercalated lattice with the platinum atoms offset by $(\frac{1}{2},0,0)$ with respect to cerium atoms. However, because of the relative positions of the bismuth atoms, the local symmetries at the cerium and platinum sites are slightly different. The Bi atoms occupy four equivalent crystallographic sites and form chains along each of the four cube diagonals, giving them a threefold axial symmetry (Fig. 2). Each Bi atom has three Ce (and Pt) nearest neighbors that form an equilateral triangle on a plane perpendicular to its axis of symmetry. These three neighbors possess their own axial local symmetry along one of the three [100], [010], [001] crystal axes (Fig. 2). These considerations mean that the principal axis of the Knight shift tensor at any of the bismuth sites coincides with and has the same symmetry as that of the electric-field tensor at the same site, which is axial along the [111] direction, referred to the z axis in the following discussions.

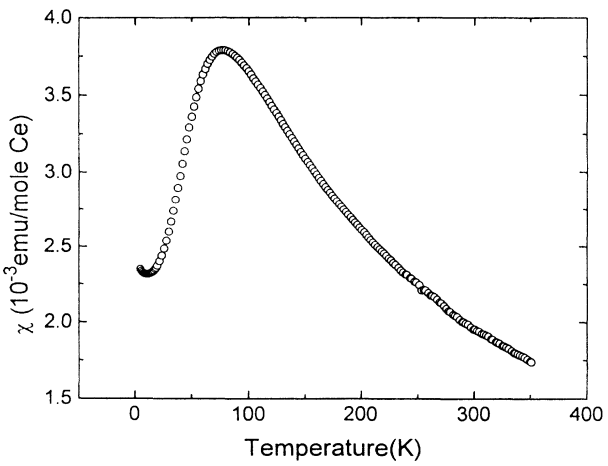

FIG. 1. Temperature dependence of the dc susceptibility for $Ce_3Bi_4Pt_3$.

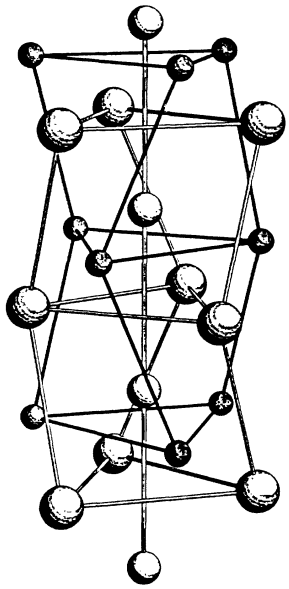

FIG. 2. The symmetry of Bi atoms along the ⟨111⟩ direction (depicted vertically). The Ce and Pt atoms are represented by the largest and smallest balls, respectively.

III. EXPERIMENTAL DATA ANALYSIS

The total Hamiltonian for nuclear spin I in magnetic field $\mathbf{H}$ with an axially symmetric electric field gradient eq is given by $H_Q + H_M$, where

$$H_Q = \tfrac{1}{2}\nu_Q[I_z^2 - I(I+1)/3 + \eta(I_+^2 + I_-^2)/6] , \quad (1a)$$

$$H_M = -\mu_N \mathbf{I}\cdot\mathbf{H} , \quad (1b)$$

where $\nu_Q = 3e^2qQ/[2I(2I-1)h]$ is the quadrupole frequency, eQ is the nuclear quadrupole moment, μ_N is the nuclear magnetic moment, and h is Planck's constant.

Zero-field ^{209}Bi ($I = \frac{9}{2}$) NQR spectra were obtained by Fourier-transforming the digitized spin echoes using a conventional pulsed NMR spectrometer. A typical spectrum has a symmetric Lorentzian line shape with a linewidth approximately 300 kHz full width at half max-

imum (FWHM). All four $\pm m \leftrightarrow \pm(m-1)$ transitions were observed and found to be at nearly exact multiples of ν_Q, consistent with the degenerate $\pm m$ levels expected from axial symmetry at the Bi sites and a vanishing asymmetry parameter η. The data are consistent with $\eta = 0.00 \pm 0.01$ throughout the temperature range studied. This finding is supported by point-charge model calculations which show that the axis of symmetry is along the [111] crystal direction, as would be expected from symmetry considerations. The NQR data thus provided an independent determination of the frequency of the nuclear quadrupole interaction without the complication of the Zeeman interaction, which is very important in the determination of the Knight shifts.

The spin-lattice relaxation rates $1/T_1$ were measured from the $\frac{5}{2} \leftrightarrow \frac{3}{2}$ and $\frac{7}{2} \leftrightarrow \frac{5}{2}$ transitions of the NQR resonance using the standard Fourier-transform spin-echo techniques, with a single saturating 90° pulse. The rf field pulses were adjusted in amplitude and width so that the bandwidth was broader than the NQR linewidth. This was carefully checked by comparing frequency-swept spectra with Fourier-transformed spectra to see that the resonance line was the same width and shape in each case. The observed magnetization recoveries were fitted to a multiexponential relaxation function,[8] consistent with a purely magnetic relaxation mechanism. The T_1 values derived from each individual transition ($\frac{5}{2} \leftrightarrow \frac{3}{2}$ and $\frac{7}{2} \leftrightarrow \frac{5}{2}$) were consistent within experimental errors. This rules out significant quadrupolar relaxation.

NMR powder spectra for ^{209}Bi were obtained by sweeping the applied external field at different temperatures between 1.8 and 300 K. A typical powder pattern for the ^{209}Bi ($I = \frac{9}{2}$) NMR spectrum at 50 MHz is shown in Fig. 3(a), in which most of the $\Delta m = \pm 1$ transitions are shown and labeled. The position of the resonance field $H_{\rm res}(m,\theta)$ for a particular transition $m \rightarrow (m-1)$ depends on the NMR Knight shift and EFG tensors, in addition to the angle θ_s where a singularity in the lineshape function occurs.[9] This singularity is given by

$$|dH_{\rm res}/d(\cos\theta)|_{\theta=\theta_s} = 0 \ , \tag{2}$$

where θ is the angle between the EFG symmetry axis and the applied field. The exact fields at which these singularities occur were determined from a line-shape simulation using a nominal set of Knight shift and EFG tensors and a Gaussian broadening [Fig. 3(b)]. The parameters were then adjusted to fit the actual data as outlined below.[10]

Once the values of $H_{\rm res}$ were determined for each transition, the Knight shift tensors were determined by exactly diagonalizing the Hamiltonian under the assumption that the shift and EFG tensors were axial with coinciding axes of symmetry. Due to the large quadrupole coupling of the Bi nuclei, perturbation theory is inapplicable. The NQR frequencies measured independently at each temperature were taken as input. Fits were made to at least three spectral peaks to maintain self-consistency. Initially, K_{xx} was calculated from the position of three 90° peaks [the $\frac{1}{2}90$, $-\frac{1}{2}90$, and $-\frac{3}{2}90$ peaks labeled in Fig. 3(b)]. Keeping K_{xx} fixed, the correct combination of K_{zz} and θ_s which fit $H_{\rm res}$ for the other transitions was determined by an iterative procedure. This final step was applied to the peaks labeled $-\frac{1}{2}56$, $-\frac{3}{2}73$, and $\frac{1}{2}37$ in Fig. 3(b). Note that both the resonant fields and the θ_s's of these peaks are strongly influenced by both K_{xx} and K_{zz}. The discontinuities at $\theta_s = 0°$ in Ce343 were too weak to be useful. For La343 the calculated tensors were verified against the $\theta_s = 0°$ peaks corresponding to $m = \frac{5}{2}, \frac{7}{2}$, and $\frac{9}{2}$.

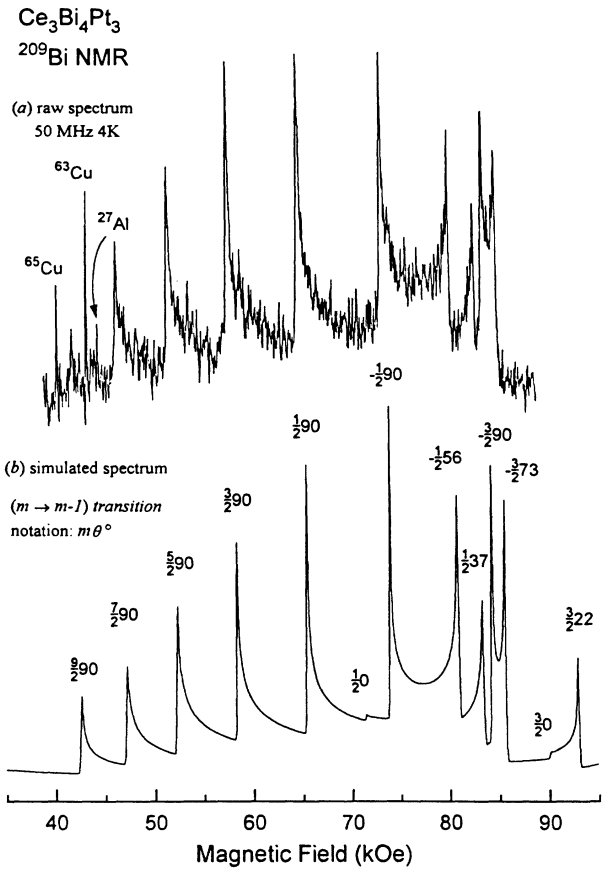

FIG. 3. (a) Quadrupolar-split ^{209}Bi NMR spectrum at 4 K and 50 MHz. (b) Simulation of the actual spectrum using NMR parameters at 4 K: $K_{xx} = K_{yy} = K_{zz} = 2.2\%$, $\nu_Q = 13.07$ MHz, and $\eta = 0$. The peaks are identified according to the θ_s and m values of a particular transition. A Gaussian broadening function of FWHM = 0.15 kOe has been convoluted with the line shape.

The spectra were very accurately described by an axially symmetric Knight shift ($K_{xx} = K_{yy}$), where the $x(y)$ and z axes are perpendicular and parallel to the external field, respectively. This axial symmetry is to be expected from the crystal symmetry, as discussed above. Finally, we note that no correction for demagnetizing fields was necessary; this error ($\leq 0.01\%$) is significantly smaller than the error introduced in determining the positions of the peaks in the NMR spectra.

IV. RESULTS AND DISCUSSION

A. Nuclear quadrupole resonance

As seen in Eq. (1), the NQR arises from the interaction between the nuclear electric quadrupole moment and the EFG at the nuclear site. A measurement of ν_Q thus provides knowledge of the spatial distribution of the charges surrounding a nuclear probe and gives insight into the electronic structure of the material.

The temperature dependences of ν_Q in Ce343 and La343 are shown in Fig. 4. For Ce343, ν_Q is constant at the lowest temperatures, rises rapidly around 30 K, and decreases at temperatures above about 100 K. The broad peak at around 80 K is about the same temperature where the peak in susceptibility is observed. In contrast, La343 has a larger value of ν_Q at all temperatures and monotonically decreases above 30 K.

Traditionally the electric quadrupole interaction has been divided between contributions from the charges in the ionic crystal lattice (ν_l) and contributions arising from the aspherical shape of the unfilled electronic orbitals (ν_e) surrounding the nucleus.[11] In such a model the quadrupole resonance frequency is then crudely written as $\nu_Q = |\nu_l \pm \nu_e|$. Written this way, it is implied that both terms incorporate antishielding contributions associated with the spatial rearrangement of the electrons in the core orbitals in response to the externally produced field gradients. The antishielding enhances the EFG at the nuclear site. It is now known that a model which distinguishes the lattice from the electronic term does not accurately reproduce either the magnitude or the temperature dependence of the measured ν_Q.[11] Rather more modern theoretical treatments calculate the EFG at the nucleus by solving Poisson's equation using self-consistent energy-band calculations for the electron wave functions throughout space. Recent calculations for hcp metals[12] demonstrate that the nonspherical distribution of valence-electron density nearest the nucleus dominates the EFG in these systems. For the hcp metals this distribution comes from the p states. In the above description this means that in the hcp metals ν_e makes a larger contribution than ν_l. While no such calculations have been carried out for Ce343, we find a similar result, as discussed below. Therefore, although we recognize the limitations of models which separate the lattice and electronic contributions of the EFG, these concepts are nevertheless useful in describing the Ce343 data.

From a point-charge model, the lattice component of ν_Q depends on the inverse cube of the distance from the charge to the probe nucleus and therefore depends sensitively on the lattice parameters. To determine the extent to which ν_l influences the temperature dependence in both samples, we plot ν_Q versus the inverse cell volume in Fig. 5. The lattice parameters are taken from neutron scattering data.[13] In Ce343, ν_Q exhibits a linear relation with the inverse volume V below about 65 K. A linear relation with $1/V$ is a signature of an ionic lattice, where the effects of the conduction electrons on the temperature dependence of the EFG are negligible. This behavior is observed in many insulators whose lattice parameters are temperature dependent.[14] Fitting the data below 65 K to a functional form given by $\nu_Q = a/V(T) + \nu_e$, we find $a = (-55.01 \pm 0.90) \times 10^3$ MHz Å^3 and $\nu_e = 68.115 \pm 0.005$ MHz. The lattice constant is about 10 Å so that the electronic term ν_e is about 25% larger than the lattice term $a/V(T)$ in Ce343 at low temperatures.

The lattice contribution for Ce343 was extrapolated to high temperatures and the data above about 100 K were fitted to a form $\nu_Q = a/V + \nu_{e0} - bT^\beta$, with a held constant at the value determined from the low-temperature fit. This fit yielded $\nu_{e0} = 68.25 \pm 0.02$ MHz, $b = 0.000\,17 \pm 0.000\,12$, and $\beta = 1.43 \pm 0.08$. Thus the nonmonotonic behavior of ν_Q versus temperature in Ce343 is due to the addition of the T^β term to ν_e (i.e., $\nu_e = \nu_{e0} - bT^\beta$ at temperatures somewhat above T_M). This is illustrated in Fig. 6. In many noncubic metals whose lattice parameters are weakly dependent on the temperature, ν_Q exhibits an empirical $-T^{3/2}$ tempera-

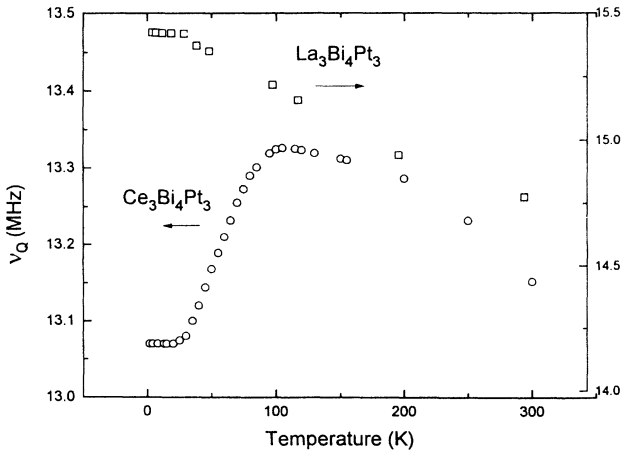

FIG. 4. Temperature dependence of the ^{209}Bi ($I = \frac{9}{2}$) NQR frequency ν_Q in $Ce_3Bi_4Pt_3$ and $La_3Bi_4Pt_3$. The data were taken from the $\frac{5}{2} \leftrightarrow \frac{3}{2}$ and $\frac{7}{2} \leftrightarrow \frac{5}{2}$ NQR resonance transitions.

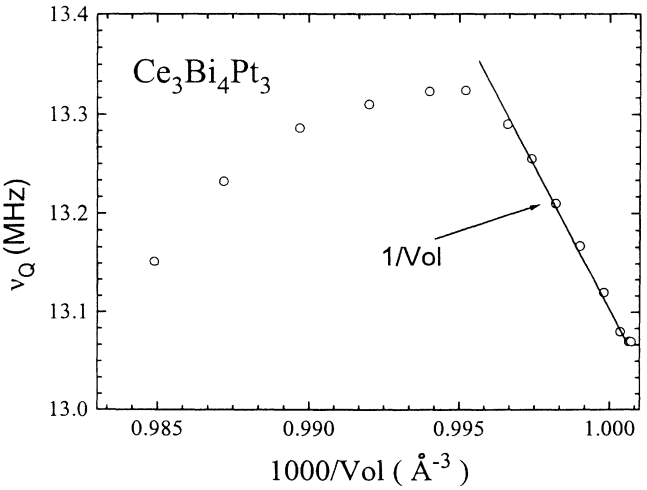

FIG. 5. NQR frequency ν_Q in $Ce_3Bi_4Pt_3$ vs inverse cell volume. The solid line is a linear fit to the low-temperature data.

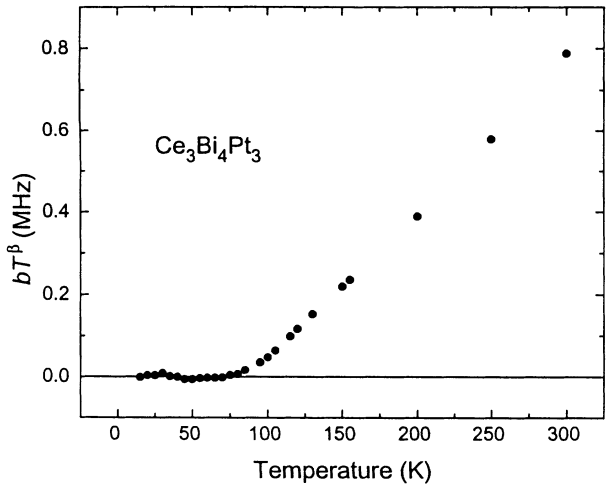

FIG. 6. Temperature dependence of the ^{209}Bi NQR frequency in $Ce_3Bi_4Pt_3$ after the volume-dependent $[a/V(T)]$ and temperature-independent terms (ν_{e0}) have been subtracted (see text). The data above about 100 K follow a $T^{3/2}$ temperature dependence characteristic of metals.

ture dependence.[11,15] This behavior has been attributed to the effects of lattice vibrations on the screened-ion pseudopotentials that give rise to the ionic component of ν_Q.[11,16] With increasing temperature the vibrational amplitudes increase and the normal-mode frequencies decrease, both tending to increase the bT^{β} term and hence decrease ν_Q.[14]

The La343 system exhibits a monotonically decreasing value of ν_Q above about 30 K, consistent with most metals. In the temperature-dependent regime, this decrease does not scale precisely with either the inverse volume or $T^{3/2}$, indicating that neither the electronic nor the lattice contributions to the EFG are dominant. We also note that ν_Q is larger in La343 than in Ce343 at all temperatures. Assuming that the electronic term is independent of the sample and ν_e is greater than ν_l, the difference in the relative signs of ν_e and ν_l in La343 and Ce343 may explain the observed data. This requires that the two contributions add in the case of La343 and be of opposite sign in Ce343, as was found above for the latter compound.

B. ^{209}Bi Knight shifts

In a paramagnetic metal, the hyperfine interaction of the conduction electrons with the nuclear spin causes a shift in the resonance field from its value in a nonmagnetic insulator, commonly referred to as the Knight shift. In this paper, we shall use the term *Knight shift* loosely to include all sources of shift in nuclear resonance and use specific qualifiers to refer to specific sources. The magnitude and anisotropy of the Knight shift, because of axial symmetry, follow the orientational dependence

$$K(\theta)=K^{\rm iso}+K^{\rm ax}(3\cos^2\theta-1)\ , \tag{3}$$

with the definitions

$$K^{\rm iso}=(K_{zz}+2K_{xx})/3 \tag{4}$$

and

$$K^{\rm ax}=(K_{zz}-K_{xx})/3\ . \tag{5}$$

Here, θ is the angle between the external field and the z axis and $K^{\rm iso}$ and $K^{\rm ax}$ are the isotropic and axial components, respectively.

In $4f$ intermetallics, where the susceptibility changes with temperature, one can separate the Knight shift into a temperature-dependent term due to the f electrons (which tracks the bulk susceptibility) and a temperature-independent term. We therefore write

$$K=K_0+K_f(T)\ , \tag{6}$$

with each piece proportional to its own component of susceptibility,

$$K_i=A_{\rm hf}(i)\chi_i/(N_A\mu_B)\ . \tag{7}$$

Here $A_{\rm hf}$ is the hyperfine coupling constant, N_A is Avogadro's number, and μ_B the Bohr magneton. K_0 represents all the temperature-independent contributions. These can be broken down into an orbital component and a contribution from the conduction-electron spins,

$$K_0=K_{\rm orb}+K_{\rm CE}\ . \tag{8}$$

The term $K_{\rm orb}$ arises from a VanVleck-like susceptibility and is generally independent of temperature, while $K_{\rm CE}$ reflects mostly the susceptibility of the conduction electrons and is only weakly temperature dependent.

Similarly, the susceptibility can be written as

$$\chi=\chi_0+\chi_f(T)\ , \tag{9}$$

where χ_0 includes the Larmor and Pauli susceptibilities from the conduction electrons and the orbital and core diamagnetism from the ions. Thus,

$$\chi_0=\chi_{\rm CE}+\chi_{\rm orb}+\chi_{\rm core}\ . \tag{10}$$

A fit to the high-temperature part of the bulk susceptibility ($T=150$–350 K) in Ce343, where $\chi_f(T)$ has a Curie-Weiss form given by $C/(T+\theta)$, yielded $\chi_0\leq 10^{-4}$ emu/mol Ce with $\theta=154\pm6$ K and an effective moment of $2.5\mu_B$. The magnitude of the χ_0 term is sample dependent and hence only an upper limit is given. We have made a rough estimate of the individual components of χ_0. The value of $\chi_{\rm CE}$ was estimated from the measured linear coefficient of specific heat γ for La343, $\gamma=10$ mJ/mol La K^2. The γ value for La343 was used because the low-temperature value of γ in Ce343 may be dominated by extrinsic effects,[3] and thus our estimate of $\chi_{\rm CE}$ is considered to be an upper limit. The value of $\chi_{\rm CE}$ was found to be about 4×10^{-4} emu/mol f.u. The orbital component is dominated by the contribution from Ce, where $\chi_{\rm orb}$ is approximately 5×10^{-5} emu/mol f.u., assuming a spin-orbit splitting of the ground state to the next higher $J=\frac{7}{2}$ multiplet levels of the order of 3000 K.[17] (We note that low-lying crystal-field levels which might produce an even larger orbital susceptibility have not been observed in Ce343, possibly due to the relatively

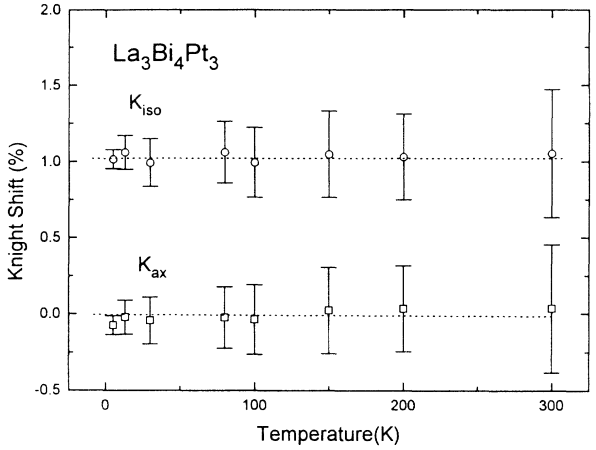

FIG. 7. Temperature dependence of the isotropic and axial Knight shifts in $La_3Bi_4Pt_3$.

strong Kondo coupling.) The core diamagnetic susceptibility can be estimated from published data[18] to be about -4×10^{-4} emu/mol f.u. Taken together the individual components of χ_0 are roughly consistent with the measured value.

Figure 7 shows the temperature dependence of the isotropic and axial Knight shifts in La343. The La compound exhibits classic metallic behavior, where the Knight shift is independent of temperature. The Knight shift values are $K^{iso}=(1.02\pm0.05)\%$ and $K^{ax}=(-0.05\pm0.05)\%$. The axial component essentially vanishes within experimental uncertainty.

By contrast with La343 the Knight shift in Ce343 exhibits a strong temperature dependence, as seen in Fig. 8. Both the axial and isotropic components are positive, and K^{ax} is about ten times smaller than K^{iso}. Each component exhibits a broad peak around 80 K, similar to the bulk susceptibility. The absence of a low-temperature tail in the Knight shift verifies that this behavior in the susceptibility is an impurity effect, as was also determined previously from neutron scattering data.[6] The fact that K^{ax} is finite in Ce343 but absent in La343 suggests that the anisotropy in Ce343 results from the f electrons of the Ce atoms.

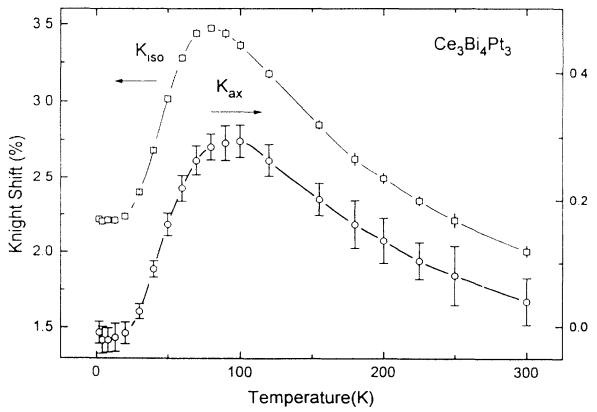

FIG. 8. Temperature dependence of the isotropic and axial Knight shifts in $Ce_3Bi_4Pt_3$. Note the $\times10$ scale for K_{ax}. For K_{iso} the errors are about the same size as the markers.

Figure 9 shows the magnitude of the Knight shift in Ce343 versus bulk susceptibility as a parametric function of temperature. Above 100 K both Knight shift components scale linearly with the susceptibility with slopes $A_f^{iso}=15.2\pm0.1$ kOe/μ_B and $A_f^{ax}=2.94\pm0.03$ kOe/μ_B. Below 80 K both components display a change in scaling with the susceptibility, which signifies a change in the electronic character of the system near this temperature. The fact that the K-χ relation is changed for both components of the Knight shift suggests a common origin for this behavior.

One may obtain the temperature-independent components of the Knight shift K_0 in Ce343 by extrapolating the measured high-temperature values to the intercept where $\chi=\chi_0$ in the K vs χ plot. The values obtained are $K_0^{iso}=(0.37\pm0.02)\%$ and $K_0^{ax}=(-0.28\pm0.01)\%$.

We now discuss the probable origin of these hyperfine fields, starting with the La343 case. The La343 Knight shift is isotropic and, as discussed below, when combined with the spin-lattice relaxation rate satisfies the Korringa relation for free electrons in a metal. We thus make the reasonable assumption that the hyperfine interaction in La343 arises predominantly from the s-band conduction electrons for which the Pauli susceptibility is dominant. From the low-temperature specific heat, we estimated the Pauli susceptibility above for La343 to be about 4×10^{-4} emu/mol f.u. Using Eq. (7) this leads to a contact hyperfine field of 1.4×10^5 Oe/μ_B. This is about 10–100 times smaller than expected for a heavy nucleus like Bi

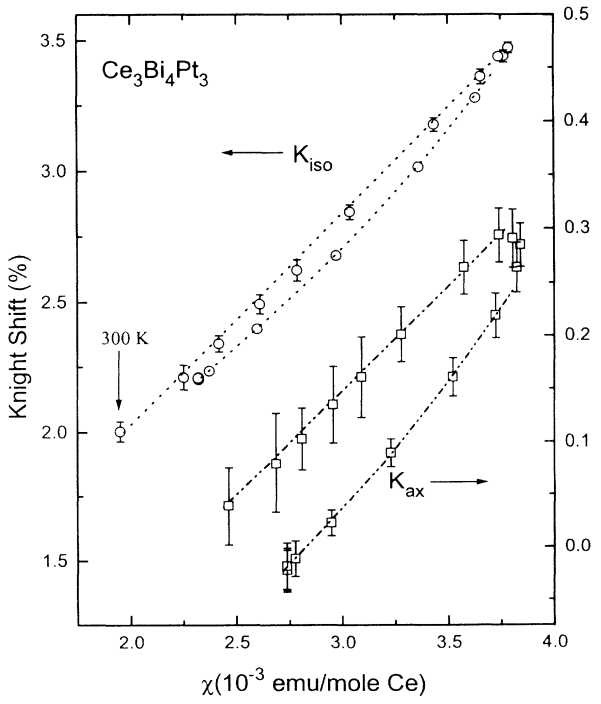

FIG. 9. Isotropic and axial Knight shifts vs bulk suceptibility with temperature as an implicit parameter. A changeover in scaling occurs at about 80 K. The lines are guides to the eye.

and most likely indicates that the density of states at the Bi site in La343 is depressed from the average value given by γ.

In Ce343 the temperature dependence of the Knight shift reflects the behavior of the susceptibility of the f electrons. Thus the hyperfine field A_f has two possible origins: a direct dipole field or a transferred hyperfine field. The dipolar hyperfine field can be calculated from the crystal structure as

$$A_f^{\rm dip} \propto \sum_i (3\cos^2\theta_i - 1)/r_i^3 , \tag{11}$$

where r_i is the distance between the Ce atom and the Bi atom. The isotropic component of $A_f^{\rm dip}$ is zero because its angular average vanishes, and hence the dipolar coupling will contribute only to $K^{\rm ax}$. Lattice-sum calculations for Ce343 show that $A_f^{\rm dip}$ is of the order of 100 Oe/μ_B, which is more than an order of magnitude smaller than the hyperfine field obtained from the $K^{\rm ax}$ vs χ plot in Fig. 9. Thus A_f must be dominated by the transferred hyperfine interaction between the Ce $4f$ orbitals and the Bi $6s$ or $6p$ orbitals.

In a metal the transferred hyperfine interaction arises from a conduction-electron-mediated exchange coupling between the f electrons and the nucleus. The Coqblin-Schreiffer model[19] for this exchange accounts for the scattering of conduction electrons in all angular-momentum channels about the f-impurity spin. This leads to an anisotropic hyperfine coupling and to a screening of both the orbital and spin components of the f moment. The latter is illustrated in Fig. 10, where the temperature dependence of the effective moment $\mu_{\rm eff}$ [proportional to $\sqrt{(\chi_f T)}$] is plotted. We derived this temperature dependence from $K_f(T)$, which is proportional to χ_f over most of the measured temperature range, ignoring the small deviation from linearity in K_f versus χ below T_M (Fig. 9). The value of K_f was used rather than χ because K_f is not seriously affected by magnetic impurities. One sees that the effective moment has decreased by a factor of at least 10 between 300 and 5 K. The residual susceptibility at $T=0$ K is likely due to a Van Vleck–like component which admixes states corresponding to the unscreened moment into the ground singlet state.

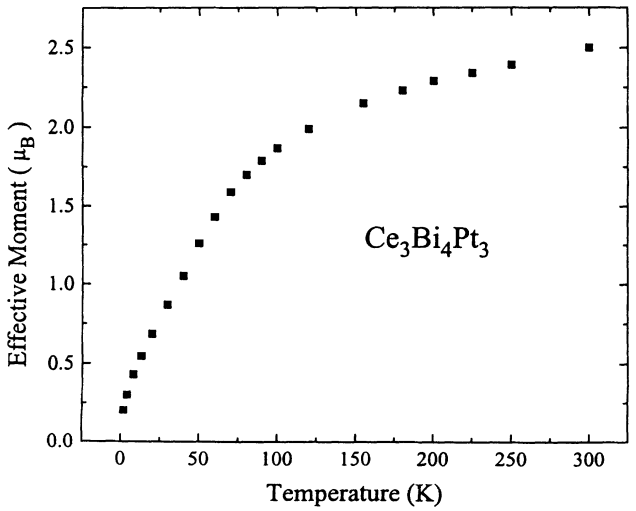

FIG. 10. Temperature dependence of the effective moment in $Ce_3Bi_4Pt_3$. The data were derived from the isotropic Knight shift and were normalized to 2.5 μ_B at 300 K (see text).

In order to make a quantitative estimate of the hyperfine coupling constant, we employ a standard analytical model[20] for the exchange Hamiltonian, which assumes an isotropic exchange coupling (in contrast to the anisotropic Coqblin-Schrieffer exchange). In this model the Hamiltonian describing the exchange between the conduction-band spin σ and $4f$ moments of spin J is given by a sum over the $4f$ sites,

$$H = -\sum_i \Gamma(i)(g_j - 1)\mathbf{J}\cdot\boldsymbol{\sigma}\delta(r_i) , \tag{12}$$

where Γ is the s-f exchange constant and g_j is the Landé g factor. In the uniform conduction-band polarization model the transferred hyperfine field is given by a spatial average of Γ, $\langle\Gamma\rangle$,

$$A_f^{\rm iso} = K_{\rm CE}\langle\Gamma\rangle(g_j - 1)/(2g_j N_A \mu_B) . \tag{13}$$

Note that for Ce, where $g_j = \frac{6}{7}$, one expects $A_f^{\rm iso}$ greater than zero if $K_{\rm CE}$ is greater than zero and $\langle\Gamma\rangle$ is less than zero. A negative $\langle\Gamma\rangle$ describes an antiferromagnetic coupling between the $4f$ moments and the conduction electrons.

We may evaluate $\langle\Gamma\rangle$ from Eq. (13) using the measured value of $A_f^{\rm iso}$ and an estimate for $K_{\rm CE}$. To obtain $K_{\rm CE}$ we must estimate $K_{\rm orb}$, or at least determine its sign [see Eq. (8)]. There are two reasonable sources for $K_{\rm orb}$: an on-site contribution from the unfilled Bi p shell and a contribution through the transferred hyperfine field from the spin-orbit splitting of the Ce $J=\frac{7}{2}$ multiplet. The first possible source can be considered negligible from the lack of anisotropy in the La343 Knight shift. (One would expect an axial component from the Bi p states.) It is difficult to estimate the magnitude of the transferred hyperfine component to $K_{\rm orb}$, but one can state that its isotropic component will be positive, as will $K_{\rm CE}$, assuming a dominant contribution from the s band. Therefore, from Eq. (8) and the measured value of $K_0^{\rm iso}$ ($\approx 0.4\%$) one may state that $K_{\rm CE} \leq 0.4\%$. This value of $K_{\rm CE}$ and the measured $A_f^{\rm iso}$ leads to a negative sign for $\langle\Gamma\rangle$ and $|\langle\Gamma\rangle| \geq 0.4$ eV. This value is consistent with other NMR measurements of the s-f coupling in rare-earth compounds.[21] We note that our estimated $|\langle\Gamma\rangle|$ is a lower limit because of our estimate for $K_{\rm CE}$ and because we have employed a model assuming a uniform conduction-electron-band polarization. Incorporation of a more realistic finite-range Ruderman-Kittel-Kasuya-Yosida (RKKY) model would lead to a larger $|\langle\Gamma\rangle|$.

The exchange model described by Eq. (12) cannot account for the observed axial component $K_f^{\rm ax}$ in the Knight shift because the model is isotropic. However, because of the axial symmetry of the three nearest-neighbor Ce atoms with respect to the Bi atoms, the Knight shift would be rendered axially symmetric even if the exchange were isotropic. Note that information re-

garding the anisotropy of the *local* Ce susceptibility cannot be obtained because of the cyclic permutation of the local Ce axis of symmetry among the three Ce neighbors. The fact that K_0^{ax} is negative requires only that K_{zz} be less than K_{xx}, which is reasonable given the planar axial geometry of the three Ce nearest neighbors.

C. Spin-lattice relaxation rates

Figure 11 shows the temperature dependence of the (isotropic) spin-lattice relaxation rate $1/T_1$ in Ce343 and La343 measured using NQR. For La343, $1/T_1$ is directly proportional to temperature over the entire temperature range and extrapolates to zero at zero temperature. This behavior is characteristic of metals. For Ce343, $1/T_1$ is proportional to temperature above about 100 K, with a slope such that $1/T_1$ also extrapolates to zero at zero temperature. Below about 100 K, however, the relaxation rate in Ce343 falls below the extrapolated linear behavior above 100 K, indicating a loss of relaxation below T_M. Defining $R=1/T_1T$ we obtain $R(\mathrm{La})=12.3$ $\mathrm{s^{-1}K^{-1}}$ and $R(\mathrm{Ce})=9.26$ $\mathrm{s^{-1}K^{-1}}$, where the value for R(Ce) is obtained for the temperature range 100–300 K.

For free-electron metals Korringa showed[22] that the spin-lattice relaxation rate and the (isotropic) Knight shift are related as follows: $R/(K^{iso})^2=\pi k_B\gamma_n^2/\mu_B^2$, where γ_n is the nuclear gyromagnetic ratio and k_B is Boltzmann's constant. For ^{209}Bi, the Korringa constant is equal to 9.85×10^4 $\mathrm{s^{-1}K^{-1}}$. Using the measured R(La) and $K^{iso}=0.01\pm0.005$, one obtains

$$R(\mathrm{La})/(K^{iso})^2=1.23\times10^5\ \mathrm{s^{-1}K^{-1}}\ ,$$

which is equal to the Korringa value within experimental error. This and the temperature dependences of the Knight shifts and relaxation rates in La343 form the basis for assuming that both are due to the conduction electrons (as discussed above for the Knight shift). We also obtain for Ce343

$$R(\mathrm{Ce})/(K^{iso})^2=5.79\times10^5\ \mathrm{s^{-1}K^{-1}}\ ,$$

a considerable enhancement over the Korringa value.

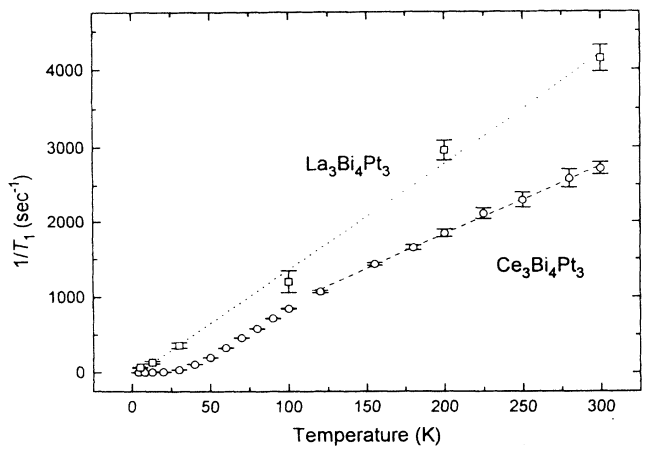

FIG. 11. Temperature dependence of the spin-lattice relaxation rate $1/T_1$ in $La_3Bi_4Pt_3$ and $Ce_3Bi_4Pt_3$.

This enhancement is attributed to the effects of the f electrons, as discussed below.

The contributions to the relaxation rate can be divided into those arising from the local f moments and from the conduction electrons at the Fermi energy: $R=R_f+R_{CE}$. In the absence of correlations, R_{CE} is proportional to the square of the density of states at the Fermi surface, $R_{CE}\sim\rho^2$, while the Knight shift is simply proportional to ρ. We can estimate the relative strengths of the conduction-electron and f contributions to the relaxation rate by comparing the results for the two compounds. To estimate R_{CE}(Ce), we take R(La) and scale it by the squared ratio of the isotropic Knight shifts,

$$R_{CE}(\mathrm{Ce})=R(\mathrm{La})[K_{CE}(\mathrm{Ce})/K^{iso}(\mathrm{La})]^2\ .$$

Because we have only an upper limit for K_{CE}(Ce) we obtain an upper limit for $R_{CE}(\mathrm{Ce})\leq2.0$ $\mathrm{s^{-1}K^{-1}}$. This yields $R_f(\mathrm{Ce})\geq7.3$ $\mathrm{s^{-1}K^{-1}}$. Hence the f electrons contribute the dominant relaxation mechanism in Ce343. The fact that R(Ce) is less than R(La) even though the f electrons add to the relaxation in Ce343 indicates that the effective densities of states for the bands producing the relaxation are reduced by the hybridization in Ce343, as already indicted by the fact that K_{CE}(Ce) is less than K^{iso}(La).

Ordinarily, local moments are not expected to produce a temperature-independent R value, as found in Ce343 at temperatures greater than 100 K. This would be expected from a Fermi liquid, which is approximated by a local-moment spin system far below its Kondo temperature. The Kondo temperature in Ce343 is estimated to be at least 300 K from the susceptibility,[3] which may be somewhat low considering that our relaxation data still show a Fermi-liquid-like behavior near this temperature.

In order to investigate the temperature dependence of the relaxation rate in Ce343 over the entire measured temperature range, we have fitted the data to a model assuming relaxation via single-particle excitations with a gapped density of states. The relaxation is related to the density of states $\rho(\varepsilon)$ at the Fermi level through

$$R\sim\int[1-f(\varepsilon)]f(\varepsilon)\rho^2d\varepsilon\ , \tag{14}$$

where $f(\varepsilon)$ is the Fermi-Dirac distribution function. The model density of states (shown in the inset of Fig. 12) allows for a constant gap to be placed at various positions relative to the center of the band, depending on the value of n. Good fits to the data were obtained for a constant spin gap of about 180 ± 10 K from 30 K up to room temperature. The best fits are for $n=0.9$ and a large bandwidth of 1600 K. The model predicts that at elevated temperatures the value of R should decrease again. Note that a bandwidth of 1600 K is an order of magnitude larger than would be predicted by the value of the Kondo temperature. This again could indicate that the actual Kondo temperature is larger than estimated previously.[3]

A good fit to the relaxation-rate data was also obtained using a recent mean-field theoretical model[23] in which the average electron occupancy of the f site increases with increasing temperature, leading to a temperature-dependent gap. These model calculations reproduce the

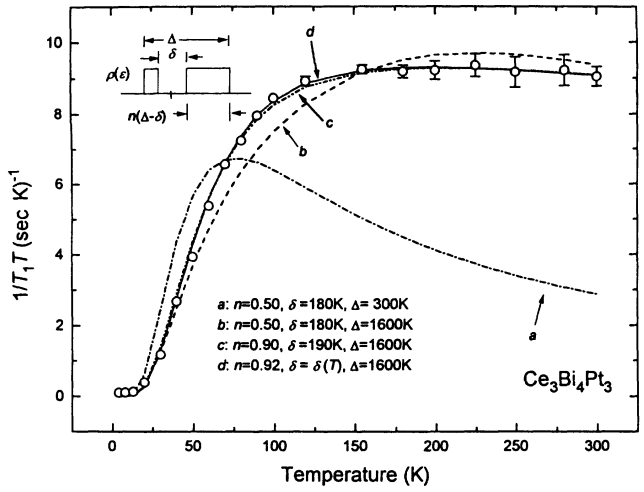

FIG. 12. Fit of $1/T_1T$ to the model density of states $\rho(\varepsilon)$ described by an energy gap of magnitude δ positioned asymmetrically with respect to the center of the band.

temperature dependence of the gap deduced from resistivity measurements[4] reasonably well. The fit to our relaxation-rate data using this temperature-dependent gap model is shown by the curve labeled $\delta(T)$ in Fig. 12. This fit yields a zero-temperature gap which is consistent with that deduced from the temperature-independent gap fits, also shown in Fig. 12 and described immediately above.

Figure 13 shows a plot of the spin-lattice relaxation rate and the model fit from Eq. (14) versus temperature in Ce343 on a log-log plot. We note that the data deviate from the model fit below about 15–20 K, indicating either relaxation from extrinsic impurities (most likely) or relaxation from intrinsic states in the gap. We cannot distinguish between these possibilities.

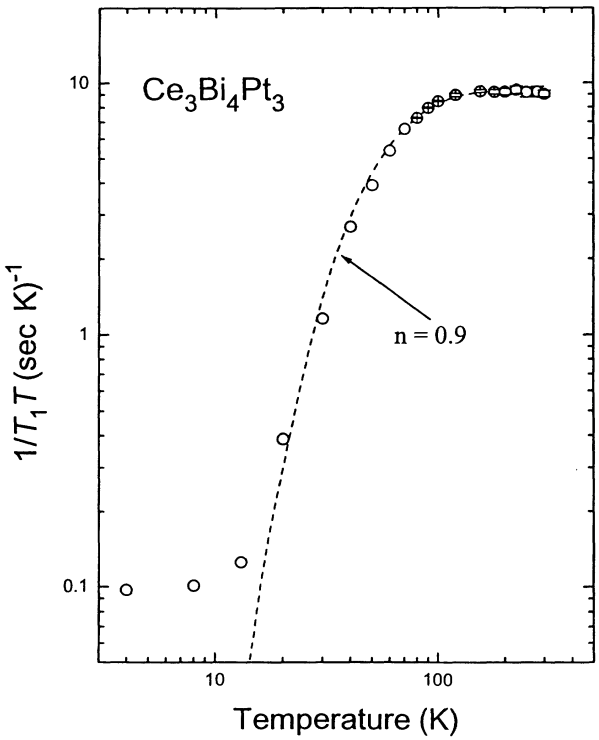

FIG. 13. Log-log plot of the spin-lattice relaxation rate $1/T_1T$ versus temperature together with the fit to the model density of states given by Eq. (14) and pictured in Fig. 12 (curves *c* and *d*).

V. CONCLUDING REMARKS

The NMR and NQR results presented in this paper have elucidated some important aspects of the static and dynamic properties of the small-gap semiconductor Ce343. The measurements of the temperature dependence of ν_Q show a dramatic change in the EFG at a nuclear site as the material goes from an insulating to a conducting state. (Previous boron NMR measurements[24,25] on YbB_{12} and SmB_6 were unable to resolve a quadrupole splitting because of the small boron quadrupole moment.) In the low-temperature insulating state the temperature dependence of ν_Q is solely determined by the lattice expansion and therefore ν_Q increases monotonically with temperature. In the high-temperature state ν_Q decreases with temperature, reflecting the onset of the typically metallic $-bT^{1.5}$ term described above. This change is presumably due to the increased effectiveness of the conduction electrons to provide long-range screening of the vibrating ionic charges in the metallic state. Because it is the low-frequency phonons (with frequencies less than the measuring temperature) which are most effective[14] in producing this characteristic metallic temperature dependence of ν_Q, our data suggest that the lattice becomes stiffer in the insulating state.

The break in the linear relation between the Knight shift and the bulk susceptibility observed in Fig. 9 has been seen before in mixed-valence materials (cf. $CeSn_3$, Ref. 26). This behavior can reflect either a change in one component of the local susceptibility to which the nuclei are most sensitive, or a change in the hyperfine coupling. Either could occur if the *s-f* hybridization changes at a characteristic temperature. It is important that the linear K-χ relation is altered for *both* K^{iso} and K^{ax}. This is because a change in K^{iso} alone could be attributed to a vanishing Pauli (χ_{CE}) susceptibility in the presence of an energy gap, thus having nothing to do with the onset of hybridization per se. (We estimate the change in K_0^{iso} from this to be $\approx 0.2\%$.) However, such an effect could not produce the observed change in K^{ax} vs χ because χ_{CE} contributes only to K_0^{iso} and not to K_0^{ax}. (Recall that K^{ax} is consistent with zero for La343.) Furthermore, because K_0^{ax} is less than zero, a decrease in K_0^{ax} would necessarily *increase* the magnitude of K^{ax}, which is contrary to what is observed below about 80 K (Fig. 9). Therefore, the NMR data strongly support the picture of a hybridization-driven gap at the Fermi surface. We have deduced a value for the magnitude of the *s-f* coupling for this hybridization which is ≥ 0.4 eV. This value is typical of hybridization in other rare-earth intermetallic compounds.

We also show that the effective moment on the Ce atoms decreases monotonically to zero as the temperature approaches zero. This is to be expected in a Kondo

system without an energy gap and, although the physics of the Kondo compensation in the presence of an energy gap is not well understood, appears to hold in this case as well.

The temperature dependence of the spin-lattice relaxation rate between 30 and 300 K in Ce343 can be adequately modeled with a spin gap of about 180 K, which either depends on temperature or is constant, and which possesses no states in the gap. The magnitude of the gap deduced from NMR is consistent with that measured via inelastic neutron scattering[6] and suggests strong coupling[2] when compared with the magnitude of the charge[5] gap (450 K). Care must be taken in making this comparison, however, because the NMR and neutron scattering are sensitive to the indirect gap, whereas the optical data may give greater weight to the direct gap. The lowest-temperature relaxation rates show a deviation from the temperature dependence predicted by the model used for the higher-temperature data, which may either be due to impurities or to intrinsic states in the gap.

Finally, one of the most striking behaviors seen in the NMR and NQR data is that all manifestations of the gap disappear at temperatures only slightly above the susceptibility maximum T_M. These effects include a change in the temperature dependence of the NQR frequency from insulating to metallic, a break in the linear relation between the Knight shift and the susceptibility, and an onset of metallic behavior in the relaxation rate. These findings are supported by neutron scattering experiments[27] on another small-gap semiconductor CeNiSn, which show that the gap in this material is destroyed by a reduction in the lifetime of the excitations near a fixed (temperature-independent) gap energy.

ACKNOWLEDGMENTS

We would like to acknowledge helpful discussions with G. Aeppli, A. J. Arko, E. T. Ahrens, C. S. Castro, P. C. Hammel, M. F. Hundley, J. M. Lawrence, D. E. Maclaughlin, M. Takigawa, S. Trugman, and H. Yasuoka. This research was performed under the auspices of the U.S. DOE, Basic Energy Sciences/DMS.

*Present address: Dept. of Physics and Astronomy, Northwestern University, Evanston, IL 60208-3112.

†Present address: Ames Laboratory, Iowa State University, Ames, IA 50011.

[1]Z. Fisk and G. Aeppli, Comments Condens. Matter Phys. **16**, 155 (1992).

[2]Z. Wang, Z.-P. Li, and D.-H. Lee, Phys. Rev. B **47**, 11 935 (1993); T. Nishino and K. Ueda, *ibid.* **47**, 12 451 (1993).

[3]M. F. Hundley, P. C. Canfield, J. D. Thompson, Z. Fisk, and J. M. Lawrence, Phys. Rev. B **42**, 6842 (1990).

[4]M. F. Hundley, P. C. Canfield, J. D. Thompson, and Z. Fisk, in *Proceedings of the International Conference on Strongly Correlated Electron Systems, San Diego, 1993* [Physica B (to be published)].

[5]B. Bucher, Z. Schlesinger, Z. Fisk, and P. C. Canfield, Phys. Rev. Lett. **72**, 522 (1994).

[6]A. Severing, J. D. Thompson, P. C. Canfield, Z. Fisk, and P. Riseborough, Phys. Rev. B **44**, 6832 (1991).

[7]P. C. Canfield and Z. Fisk, Philos. Mag. B **65**, 1117 (1992).

[8]A. Narath, Phys. Rev. **162**, 320 (1967); D. E. MacLaughlin, J. D. Williamson, and J. Butterworth, Phys. Rev. B **4**, 60 (1971).

[9]M. H. Cohen and F. Reif, in *Solid State Physics: Advances in Research and Applications,* edited by F. Sietz and D. Turnbull (Academic, New York, 1957), Vol. 5, p. 321.

[10]Because of the broadening, the positions of the singularities do not correspond with the apparent peaks in the actual spectrum but are located at positions which are 70–90 % of the peak heights, depending upon which transition is observed.

[11]E. N. Kaufmann and R. J. Vianden, Rev. Mod. Phys. **51**, 161 (1979).

[12]P. Blaha, K. Schwartz, and P. H. Dederichs, Phys. Rev. B **37**, 2792 (1988).

[13]G. H. Kwei, J. M. Lawrence, P. C. Canfield, W. P. Beyermann, J. D. Thompson, Z. Fisk, A. C. Lawson, and J. A. Goldstone, Phys. Rev. B **46**, 8067 (1992).

[14]T. Kushida, G. B. Benedek and N. Bloembergen, Phys. Rev. **104**, 1364 (1956).

[15]J. Christiansen, P. Heubes, R. Keitel, W. Klinger, W. Loeffer, W. Sandner, and W. Witthuhn, Z. Phys. B **24**, 177 (1976).

[16]K. Nishiyama, F. Dimmling, Th. Kornrumpf, and D. Riegel, Phys. Rev. Lett. **37**, 357 (1976); P. Jena, Phys. Rev. Lett. **36**, 418 (1976).

[17]R. J. Elliot, *Magnetic Properties of Rare Earth Metals* (Plenum, New York, 1972).

[18]S. Fraga, K. Karwowski, and K. M. S. Saxena, *Handbook of Atomic Data* (Elsevier, Amsterdam, 1976).

[19]B. Coqblin and J. R. Schrieffer, Phys. Rev. **185**, 847 (1969).

[20]V. Jaccarino, B. T. Matthias, M. Peter, H. Suhl, and J. H. Wernick, Phys. Rev. Lett. **5**, 251 (1960).

[21]E. D. Jones, Phys. Rev. **180**, 455 (1969); H. W. de Wijn, K .H. J. Buschow, and A. M. van Diepen, Phys. Status Solidi **30**, 759 (1968).

[22]J. Korrina, Physica **16**, 601 (1950).

[23]C. Sanchez-Castro, K. S. Bedell, and B. R. Cooper, Phys. Rev. B **47**, 6879 (1993); see also P. S. Riseborough, *ibid.* **45**, 13 984 (1992).

[24]M. Kasaya, F. Iga, M. Takigawa, and T. Kasuya, J. Magn. Magn. Mater. **47&48**, 429 (1985).

[25]M. Takigawa, H. Yasuoka, Y. Kitaoka, T. Tanaka, H. Nozaki, and Y. Ishizawa, J. Phys. Soc. Jpn. **50**, 2525 (1981).

[26]D. E. MacLaughlin, J. Magn. Magn. Mater. **47&48**, 121 (1985).

[27]T. E. Mason, G. Aeppli, A. P. Ramirez, K. N. Clausen, C. Broholm, N. Stucheli, E. Bucher, and T. T. M. Palstra, Phys. Rev. Lett. **69**, 490 (1992).

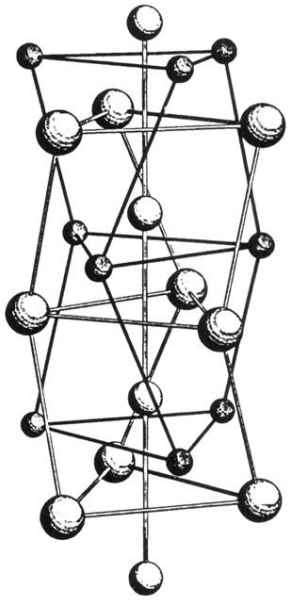

FIG. 2. The symmetry of Bi atoms along the ⟨111⟩ direction (depicted vertically). The Ce and Pt atoms are represented by the largest and smallest balls, respectively.